

## Article

# Electron Transport in *n*-Type InSe van der Waals Crystals with Co Impurities

Zakhar R. Kudrynskiy <sup>1,2,\*</sup> , Illya V. Mintyanskii <sup>2</sup>, Petro I. Savitskii <sup>2</sup> and Zakhar D. Kovalyuk <sup>2</sup>

<sup>1</sup> Advanced Materials Research Group, Faculty of Engineering, University of Nottingham, Nottingham NG7 2RD, UK

<sup>2</sup> I.M. Frantsevich Institute for Problems of Materials Science, National Academy of Sciences of Ukraine, Chernivtsi Branch, 58001 Chernivtsi, Ukraine

\* Correspondence: zakhar.kudrynskiy@nottingham.ac.uk

**Abstract:** Intercalation and doping are promising routes to tune properties of van der Waals (vdW) semiconductors and pave the way for their applications in digital electronics beyond Moore's law, sensors and spintronics. The indium selenide (InSe) vdW crystal shows great promise for use in next-generation semiconductor technologies. For these applications to be realized, the effects of impurities on properties of InSe must be understood. Here, we present a comparative experimental study of electron transport in *n*-type InSe semiconductor doped and electrochemically intercalated with magnetic cobalt (Co) impurities. It is shown that the presence of Co decreases the free electron density, the Hall mobility along layers and the conductivity anisotropy  $\sigma_{\perp C}/\sigma_{\parallel C}$ . Furthermore, this leads to a change of the behavior of  $\sigma_{\perp C}(T)$  dependence from a metallic one in pristine samples to a semiconducting one in samples with Co. We also demonstrate that the interaction of electrons with space-charge regions is an effective scattering mechanism, which should be taken into account in doped and intercalated crystals. The present work is important for the basic physics knowledge of the effect of Co impurities on physical properties of InSe, which is needed to tailor the parameters of this semiconductor for applications in electronics and spintronics.

**Keywords:** InSe; electron transport; semiconductors; van der Waals crystals; intercalation; doping; cobalt; magnetic impurities



**Citation:** Kudrynskiy, Z.R.; Mintyanskii, I.V.; Savitskii, P.I.; Kovalyuk, Z.D. Electron Transport in *n*-Type InSe van der Waals Crystals with Co Impurities. *Appl. Sci.* **2022**, *12*, 9932. <https://doi.org/10.3390/app12199932>

Academic Editor: Filippo Giannazzo

Received: 5 September 2022

Accepted: 27 September 2022

Published: 2 October 2022

**Publisher's Note:** MDPI stays neutral with regard to jurisdictional claims in published maps and institutional affiliations.



**Copyright:** © 2022 by the authors. Licensee MDPI, Basel, Switzerland. This article is an open access article distributed under the terms and conditions of the Creative Commons Attribution (CC BY) license (<https://creativecommons.org/licenses/by/4.0/>).

## 1. Introduction

For several decades, conventional semiconductor materials, mainly silicon (Si) and III-V compounds, such as gallium arsenide (GaAs), gallium nitride (GaN), etc., have been at the center of condensed matter physics research and many important technologies. However, since traditional Si-based technologies are reaching the scaling limit, researchers all over the world are looking for a novel class of semiconductor materials, which can create new routes to the next-generation digital electronics beyond Moore's law, spintronics and quantum optics for fast, secure communications, and quantum detection.

In recent years, the search for new transformative materials has led to the rapidly growing development of two-dimensional (2D) van der Waals crystals thanks to their promising electronic, optical and thermoelectric properties [1,2]. These novel materials promise to be a disruptive technology in next generation transistors, sensors, light-emitting diodes, power sources, etc. [2]. Amongst the wide library of 2D van der Waals materials, indium selenide (InSe) has emerged as a very promising semiconductor, which is well suited for various applications, including but not limited to transistors, photodetectors, THz detectors, optical modulators, quantum metrology, flexible nano-photonics and thermoelectric technologies [3–13]. An interesting aspect of current research is the controlled manipulation of the spin and charge of electrons in 2D van der Waals semiconductors. This can create new routes to spintronics, which would require the development of magnetic nanostructured

materials that integrate both semiconducting and magnetic properties within the same crystal. To date, the integration of magnetic properties within a semiconductor crystal has proven to be challenging. Attempts to create magnetic semiconductors have often led to a significant deterioration of the crystal quality, but also led to material systems with new interesting magnetic and electronic properties.

The majority of layered van der Waals materials, including InSe, are nonmagnetic in the pristine form, which restricts their application in spintronic devices, and controlling their magnetism still remains an open question [14]. The integration of magnetic properties within a semiconductor van der Waals crystal is generally challenging to achieve. This integration is important for several applications and new device concepts in spintronics, including electrical control of the magnetization and generation of spin-currents, spin-filtering and spin-amplification in logic devices. To date, the realization of magnetic semiconductors has proven to be challenging, but it has a great potential to lead to material systems with interesting magnetic and electronic properties.

There are many ways to introduce magnetism in such layered materials, for instance by using dopants, vacancies, elastic deformations and absorption of molecules [15]. In contrast to conventional covalently bonded materials, the properties of van der Waals crystals can be changed by one more method, namely intercalation [16]. The absence of dangling bonds within separate layers of III-VI crystals and a significant spacing between them ( $3\div 4$  Å) enable modification of properties of as-grown crystals by inserting guest species, such as atoms, ions or molecules, into empty van der Waals gaps. Their number can be compared and even exceed that of the basic compound. Intercalation technology enables creation of new composite material systems in which there is a nanoscale alternation of semiconductor 2D layers and intercalant interlayers, including those of magnetic substances. This has been explored in our earlier experiments on III-VI van der Waals compounds [17–22]. This approach can be considered as one of the most promising for progress of spintronic devices based on van der Waals semiconductors.

Previous attempts to obtain semi-magnetic van der Waals III-VI semiconductors reported in the literature usually involved adding magnetic dopants before synthesis [23–28]. These earlier works indicated that along with the crystallization of layered crystals, the formation of additional embedded clusters and ferromagnetic ordering takes place. In contrast to many conventional semiconductors, electronic, optical and vibrational properties of these compounds are mostly preserved after adding magnetic dopants [26]. Moreover, a high uniaxial magnetic anisotropy with magnetization oriented across the layers along with the occurrence of ferromagnetic properties with Curie temperature above room temperature reveal possibilities for development of next-generation functional devices, combining magnetic and semiconductor properties in the same material, and stimulate further investigations [26]. It should be noted that magnetic clusters are 2D and oriented along the layers with a nanoscale dimension across the layers.

Hybrid systems consisting of magnetic inclusions and van der Waals III-VI semiconductors have been investigated by various methods including resonance and X-ray techniques, neutron diffraction, impedance spectroscopy, electron microscopy, optical methods, etc. [23,25,26,28]. However, the electrical properties of these novel material systems remain largely unexplored, hindering further exploitation of these materials in electronics and spintronics. There are very few publications on this topic, and they are mainly limited to investigation of the electrical conductivity of *n*-type InSe samples with various magnetic impurities [20,23,27]. In this work, we present a study on the effect of magnetic Co impurities on direct current (d.c.) electrical parameters of InSe and their anisotropy. Samples for investigation of the magnetic semiconductor were obtained both by adding the dopant before synthesis of the compound and by intercalation of previously grown nominally undoped InSe crystals.

## 2. Materials and Methods

*Crystal growth.* Nominally undoped InSe single crystals were grown by the Bridgman method from an indium-rich melt of components with a nonstoichiometric composition of  $\text{In}_{1.03}\text{Se}_{0.97}$ . This facilitates the formation of indium-interstitial atoms which act as native donors and lead to  $n$ -type conductivity.

To obtain a homogeneous ferromagnetic semiconductor system based on In-Se, we have explored different methods for incorporating transition metals in InSe material. These methods involve the incorporation of the transition metals (namely Co in this study) during the Bridgman growth or the intercalation of the transition metals after the growth of InSe. These methods are described below.

*Doping.* The Co dopant was introduced by adding 10 at. % of high-purity (99.999%) Co to the initial load. Since the Co melting point is high (1495 °C), for the doped ingot the temperature and duration of synthesis, 1000 °C and two weeks, respectively, were higher than for undoped InSe. It is known that the solubility of dopants in indium monoselenide is very low and most of that is pushed towards the end of ingots when growing layered van der Waals crystals. It means that the nominal amount of a dopant and its real content in different parts of an ingot can be essentially different. For this reason, the Co distribution along the ingot was determined for several pieces of the sample by means of X-ray fluorescence analysis, which revealed that it is inhomogeneous. For electrical measurements, we selected pieces of the ingot with the following composition  $\text{Co}_{0.12}\text{InSe}$ .

*Intercalation.* Significantly smaller ionic radius of double-charged  $\text{Co}^{2+}$  ions (0.78 Å) compared to the interlayer separation of InSe sheets (3.8 Å) enables to perform their intercalation into the van der Waals gaps [29]. The electrochemical insertion of Co ions was carried out by using a method of “drawing” electrical field under galvanostatic conditions. As electrolyte we used a saturated aqueous solution of cobalt sulphate  $\text{CoSO}_4$  providing a low current density (0.2 mA/cm<sup>2</sup>) through intercalated samples. The required amount of the ions ( $x = 0.12$  in  $\text{Co}_x\text{InSe}$ ) was calculated according to the Faraday’s law and regulated with the amount of transferred electric charge.

*Structural studies.* X-ray diffraction studies were performed by means of a DRON-3 X-ray diffractometer with a monochromatic Cu-K $\alpha$  radiation of wavelength  $\lambda = 1.5418$  Å. LATTIK–KARTA software was used to analyze the obtained X-ray diffraction patterns.

*Surface morphology studies.* Image acquisitions were performed using a field-emission gun scanning electron microscope (JEOL 7100 FEG-SEM). Prior to studies of surface morphology, the crystals were freshly cleaved to avoid oxidation and degradation over time at ambient conditions.

*Photoluminescence measurements.* The excitation of photoluminescence spectra was done using a current-wave semiconductor laser with  $\lambda = 532$  nm ( $p = 100$  mW) equipped by a laser (SL-532-10 Thorlabs) and edge (LP-03-532-RS Semrock’s) filters. The experimental set-up for photoluminescence measurements comprised a 0.6 m optical spectrometer MDR-23 (LOMO) with a grating of 600 groves/mm.

*Electrical measurements.* The samples for measurements of electrical conductivity in different crystallographic directions and the Hall effect were prepared using plane-parallel plates mechanically cleaved from the as-grown InSe crystal ingots. It is worth noting that the as-cleaved InSe (0001) surfaces are atomically smooth and do not require any additional chemical or mechanical treatment for electrical and optical applications. After characterization of electrical properties of pristine samples, they were subjected to intercalation with  $\text{Co}^{2+}$  ions. The investigation of the temperature dependence of the in-plane electrical conductivity,  $\sigma_{\perp C}$ , i.e., along the layers of a van der Waals crystal, and the Hall coefficient ( $R_H$ ) in the range of temperature ( $T$ ) from  $T = 80$  K to 400 K were conducted for InSe samples with rectangular parallelepiped shape and typical sizes of  $0.8 \times 2.5 \times 10$  mm<sup>3</sup> at direct current applied through the samples and under a constant magnetic field. It should be noted that the electrical properties of the pristine and intercalated  $n$ -type InSe crystal were investigated for the same sample. As a contact material we used high purity metallic in-

dium (In) which provides a good ohmic contact to *n*-type InSe. The contacts were prepared using a soldering iron.

The mechanical properties and the layered crystal structure of InSe with the weak interlayer interactions make possible preparation of samples with dominant dimension across the layers. Namely, van der Waals crystals can be easily mechanically cleaved along the (0001) planes. Therefore, to measure vertical conductivity,  $\sigma_{\parallel C}$ , we used a four-probe method. Typically, their in-plane dimensions were  $\sim 5 \times 3 \text{ mm}^2$ , and thickness was  $\sim 0.6 \text{ mm}$ . The contacts were prepared on the cleaved surfaces of the InSe samples normal to the *C* crystallographic axis. The current contacts were deposited in such a way that they covered almost all the surface on each side. The Hall voltage was measured using a pair of smaller probe contacts located closely to the current electrodes. The distance between the current and the probe electrodes on each side did not exceed 0.5 mm. The measurements of the out-of-plane, i.e., vertical electrical conductivity were performed in the range of temperatures from  $T = 80 \text{ K}$  to  $300 \text{ K}$ .

### 3. Results and Discussion

#### 3.1. Crystal Structure, Surface Morphology and Optical Properties

The  $\gamma$ -phase InSe (R3m space group) and Co-doped  $\gamma$ -InSe single crystals were synthesized using the Bridgman method of crystal growth from a polycrystalline melt of  $\text{In}_{1.03}\text{Se}_{0.97}$ . Co-dopants were introduced during the growth at a nominal concentration of 10% (see Materials and Methods). The rhombohedral unit cell of  $\gamma$ -InSe has lattice parameters  $a = b = 4.002 \text{ \AA}$  and  $c = 24.961 \text{ \AA}$ . The primitive unit cell of this crystal consists of three van der Waals layers. Each of these layers has a thickness of  $L = 0.8320 \text{ nm}$  (i.e., 1 stoichiometric layer) and contains four covalently bonded monoatomic sheets with the following sequence Se–In–In–Se. The atoms form hexagons within each plane. The layers interact by weak van der Waals forces leading to anisotropic electronic properties and can be mechanically cleaved. The performed X-ray diffraction measurements (Figure 1) revealed that the lattice parameters of the InSe samples were weakly modified by doping and intercalation with Co (Table 1).

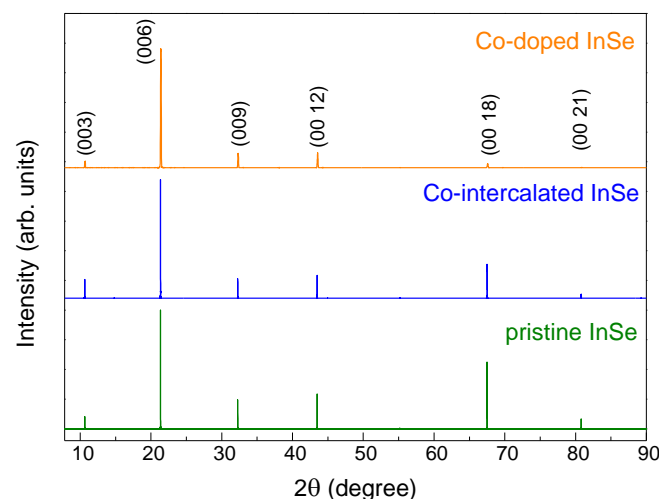


**Figure 1.** X-ray diffraction patterns recorded for InSe samples: as-grown pristine, Co-intercalated and Co-doped.

**Table 1.** Lattice parameters (*a*, *b* and *c*) from the X-ray diffraction studies of the InSe samples.

Samples	$a = b \text{ (\AA)}$	$c \text{ (\AA)}$
Pristine InSe	$4.002 \pm 0.003$	$24.950 \pm 0.012$
Co-intercalated	$4.003 \pm 0.006$	$24.952 \pm 0.002$
Co-doped InSe	$4.012 \pm 0.015$	$24.908 \pm 0.022$

Our studies reveal that the optical properties of InSe are largely preserved in the samples with Co impurities. Namely, the energy peak positions of the room temperature ( $T = 300$  K) photoluminescence emission for the intercalated and doped samples are centered at the same energy  $h\nu = 1.25$  eV as for the pristine bulk InSe (Figure 2). As could be expected, the intensity of the optical signal in InSe samples with Co impurities is lower than in the pristine one and is nonhomogeneous over length scales of several micrometers, but, remarkably, this semiconductor material remains optically active even with a high concentration of impurities. These attractive optical properties of the InSe semiconductor with magnetic impurities can open up a new avenue in material design offering innovative solutions for optoelectronics.

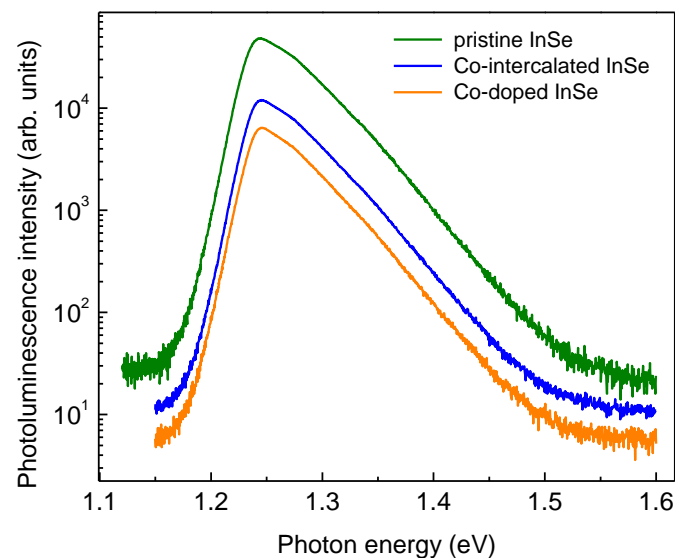


**Figure 2.** Photoluminescence spectra of bulk InSe samples measured with the excitation laser wavelength of 532 nm ( $p = 100$  mW) at  $T = 300$  K for: as-grown pristine, Co-intercalated and Co-doped InSe crystals.

Freshly cleaved surfaces of InSe samples were imaged using scanning electron microscopy (Figure 3). Figure 3a,b show smooth and defect-free van der Waals surfaces of pristine and Co-intercalated InSe, respectively. In contrast to those, image of the cleaved surface of Co-doped InSe shown in Figure 3c reveals nonuniform surface over the scale of hundreds of nanometers, which indicates that the large amount of Co impurities in  $\text{Co}_{0.12}\text{InSe}$  causes a slight distortion of crystal structure resulting in defects, such as regions with misoriented layer planes.

### 3.2. Electrical Properties along InSe Layers

We show the recorded temperature dependences of the in-plane electrical conductivity  $\sigma_{\perp C}$  (Figure 4), the in-plane electron Hall mobility  $\mu_{\perp C}$ , i.e., along the layers, (Figure 5), and the Hall coefficient  $R_H$  (Figure 6) for the pristine as-grown, intercalated and doped with cobalt InSe van der Waals samples. Table 2 shows the corresponding numerical values. It was revealed that in the case of the initial sample at low temperatures the measured Hall coefficient decreases with an increase in temperature. Such behavior is caused by a shallow, mostly ionized even at  $T = 80$  K, donor level (18.5 meV) arising from interstitial  $\text{In}_i$  atoms [30]. High values of the mobility indicate high quality of the samples, and the decrease in  $\mu_{\perp C}$  with increasing temperature takes place because the electron-phonon interaction is the dominant scattering mechanism. This behavior of Hall coefficient  $R_H$  and electron Hall mobility  $\mu_{\perp C}$  determines a metallic temperature dependence of the in-plane electrical conductivity component  $\sigma_{\perp C}$  at  $T < 380$  K. However, at higher temperatures the electron density strongly increases due the activation of electrons from deeper donor states leading to a typically semiconductor  $\sigma_{\perp C}(T)$  dependence.

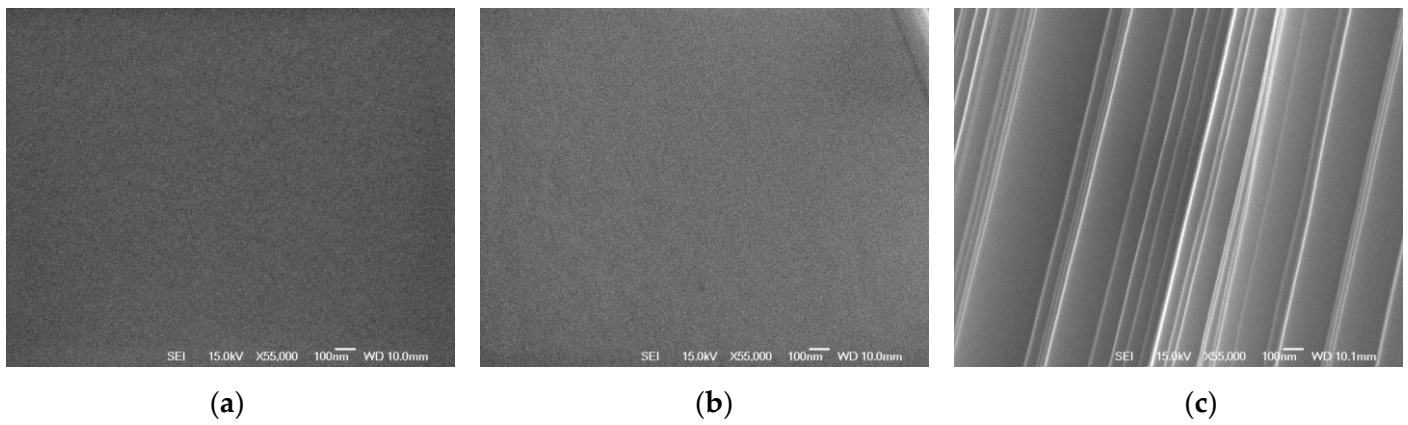


**Figure 3.** Scanning electron microscope micrographs showing cleaved surfaces of (a) as-grown pristine, (b) Co-intercalated and (c) Co-doped InSe crystals.

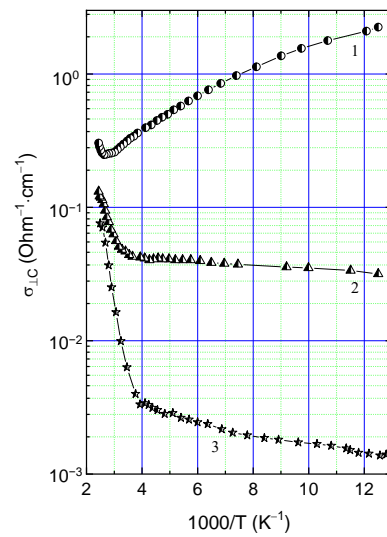


**Figure 4.** The in-plane electrical conductivity versus temperature for as-grown pristine (1), Co-intercalated (2) and Co-doped (3) *n*-type InSe crystals.

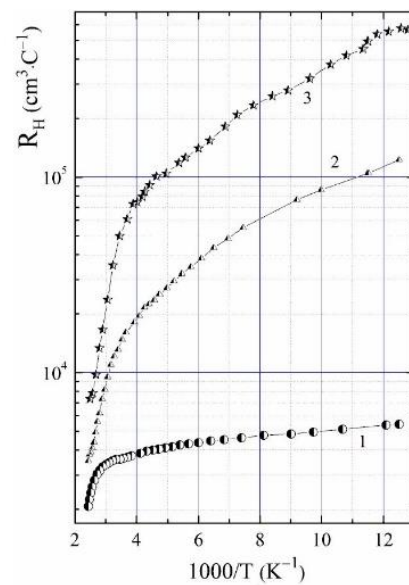


**Figure 5.** The Hall coefficient versus temperature for as-grown pristine (1), Co-intercalated (2) and Co-doped (3) *n*-type InSe crystals.

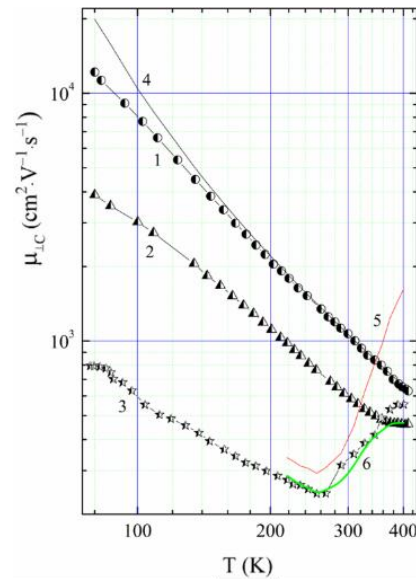


**Figure 6.** The in-plane mobility versus temperature for as-grown pristine (1), Co-intercalated (2), and Co-doped (3) *n*-type InSe crystals; calculated curves: 4– $\mu_{FS}(T)$ , 5– $\mu_{SCR}(T)$  and 6–total mobility.

**Table 2.** In-plane electrical properties of various *n*-type InSe samples.

Sample No	Type of Sample	$\sigma_{\perp C}$ , $\text{Ohm}^{-1} \cdot \text{cm}^{-1}$		$n$ , $\text{cm}^{-3}$		$\mu_{\perp C}$ , $\text{cm}^2 \cdot \text{V}^{-1} \cdot \text{s}^{-1}$	
		80 K	300 K	80 K	300 K	80 K	300 K
1	Undoped	2.243	0.298	$1.15 \times 10^{15}$	$1.74 \times 10^{15}$	12,180	1070
2	Co-intercalated	$3.17 \times 10^{-2}$	$4.82 \times 10^{-2}$	$5.09 \times 10^{13}$	$5.16 \times 10^{14}$	3890	584
3	Co-doped	$1.38 \times 10^{-3}$	$9.92 \times 10^{-3}$	$1.09 \times 10^{13}$	$1.77 \times 10^{14}$	794	350

According to the previous theoretical studies on electron-lattice interaction in layered semiconductors reported in the literature [31], the scattering of charge carriers with homopolar optical phonons, which are polarized along the C crystallographic axis (i.e., out-of-plane) and which modulate the thickness of separate layers, is prevailing in layered van der Waals crystals. In this case, the relaxation time can be expressed as following:

$$1/\tau_{FS} = 2g^2\omega \left[ ((\epsilon/\hbar\omega) + 1)^{1/2}n_{ph} + (n_{ph} + 1)\Theta(\epsilon - \hbar\omega)((\epsilon/\hbar\omega) - 1)^{1/2} \right] \quad (1)$$

Here  $g^2 = \epsilon_0^2 m^{*3/2} MN\hbar(\hbar\omega)^{3/2}$  defines the electron-phonon coupling constant,  $\hbar\omega$  defines the energy of the phonon,  $\epsilon_0$  defines the deformation potential per unit displacement with respect to the normal coordinate of the phonon mode,  $N$  defines the number of cells per unit volume,  $M$  defines the reduced ionic mass of the phonon mode,  $\epsilon$  defines the electron energy,  $n_{ph} = [\exp(\hbar\omega/kT) - 1]^{-1}$  defines the phonon occupation number,  $m^* = (m_{\perp C}^{*2} m_{\parallel C}^*)^{1/3}$  defines the density-of-states effective mass and  $\theta(x)$  is equal to unity at  $x \geq 0$  and is 0 at  $x < 0$ . In the 3D approach, taking into account the scattering with homopolar optical phonon  $A'_{1g}$  ( $\hbar\omega = 14.3$  meV) and  $g_2 = 0.051$  the mobility temperature dependence  $\mu_{FS}(T)$  has a form shown by the curve 4 in Figure 6. In this case, the slight deviation of the apparent mobility from the phonon one at low temperature for the pristine InSe sample can be interpreted taking into account additional scattering with the ionized impurities. Thus, by expressing the total mobility as  $\mu^{-1} = \mu_{FS}^{-1} + \mu_{BH}^{-1}$  and presuming that in the Brooks–Herring relationship for impurity scattering the effective density of screening charge carriers equals to the density of the free electrons, we have obtained the following values  $N_i = 4.37 \times 10^{15} \text{ cm}^{-3}$ ,  $N_d = 2.76 \times 10^{15} \text{ cm}^{-3}$  and  $N_a = 1.61 \times 10^{15} \text{ cm}^{-3}$  for the pristine sample at  $T = 80$  K. Here  $N_i$ ,  $N_d$  and  $N_a$  are the densities of ions, donors

and acceptors, respectively. This indicates that the as-grown pristine InSe crystal is not a heavily compensated semiconductor material.

Doping and intercalation of *n*-type InSe with Co also affects the  $n(T)$  dependence leading to a decrease in the free electron density. This effect is more pronounced in the low-temperature range. At  $T = 80$  K the value of  $n$  is two and nearly twenty orders of magnitude smaller for the doped and intercalated samples, respectively, than for the pristine one. At the highest temperatures, the values of all the Hall coefficients are quite close. For both samples with Co impurities the  $\sigma_{\perp C}$  variation over the whole temperature range exhibits semiconductor behavior with substantially lower values. Adding Co impurities also leads to a significant decrease in the in-plane electron Hall mobility (i.e., along the layers) and the emergence of non-monotonous high-temperature peculiarities in its variation. For the pristine samples, in the low-temperature range the mobility decreases with increasing temperature, i.e., there is no tendency to create a maximum. It means that even at liquid nitrogen temperature the transition to dominant scattering with charged impurities is not observed. The apparent  $\mu_{\perp C}(T)$  temperature dependence for the intercalated and doped samples at high temperatures indicates that it is important to take into account an additional scattering mechanism for electrons in this range. As an important mechanism for InSe, we can consider scattering with space-charge regions (SCR) [32,33]. When the SCR radius is less than the free path of electrons these regions act as scattering centers. Assuming that free carriers cannot penetrate into them, the expression for mobility has the following form [34]:

$$\mu_{SCR} = \frac{e}{(2m^*kT)^{1/2}N_{SCR} \cdot S} \quad (2)$$

Here  $N_{SCR}$  defines the density of space-charge regions and  $S$  is the corresponding effective cross-section. Assuming that  $S \sim r_D^2$  where the Debye screening radius is  $r_D = \left(\frac{ekT}{4\pi e^2 n}\right)^{1/2}$ , the expression for  $\mu_{SCR}$  takes a form of

$$\mu_{SCR} = \frac{4e^3}{\epsilon(2m^*)^{1/2}k^{3/2}} \frac{1}{N_{SCR}} nT^{-3/2} \equiv \frac{B}{N_{SCR}} nT^{-3/2} \quad (3)$$

Then, taking into account the additional ionized impurity scattering, we can express the total mobility as following:

$$\mu^{-1} = \mu_{ph}^{-1} + \mu_{BH}^{-1} + \mu_{SCR}^{-1} \quad (4)$$

In the interlayer spaces of *n*-type InSe the intercalated Co can be distributed uniformly and occupy energetically favorable octahedral and tetrahedral sites between the Se planes of adjacent layers or create ferromagnetic Co-islands (clusters) embedded into rhombohedral  $\gamma$ -polytype InSe crystal and randomly distributed over the layer plane. Such inclusions in a low-resistive layered crystal may act as an additional scattering mechanism of free electrons and decrease the in-plane Hall mobility by more than a factor of three at  $T = 80$  K.

At the same time, in the doped crystal the effect of the interaction with space-charge regions appears to be far stronger, namely at the lowest temperature the mobility decreased by a factor of about 15, and in the high temperature range  $\mu_{\perp C}$  abruptly increases with increasing  $T$ . It is known from the paper [23] that in InSe < Mn > material there are two different impurity subsystems which is confirmed by the existence of two lines in the spectra of electron paramagnetic resonance. Co-doped atoms can also agglomerate and form small islands between InSe layers as well as enter ionic-covalent layers occupying In or Se sites, to be interstitials or to aggregate into clusters randomly distributed in the bulk of the semiconductor. As noted in [24], for spintronic materials an inhomogeneous (cluster) structure is rather a rule than an exception. Hence, inhomogeneous spatial distribution of the magnetic dopant in InSe and the presence of ferromagnetic inclusions lead to additional scattering of electrons. An abrupt increase in free electron density, apparent at high temperatures for the doped semiconductor (Figure 5), causes the increase in the  $\mu_{SCR}$  component

and the total mobility becomes closer and closer to the lattice induced mobility when the temperature increases. Thus, in the high-temperature range we can neglect the ionized impurity scattering. Hence, we can determine the  $\mu_{\text{SCR}}$  component from expression (4) and the density  $N_{\text{SCR}}$ , which equals  $3.26 \times 10^{14} \text{ cm}^{-3}$  for sample 3, from expression (3), and plot the  $\mu_{\text{SCR}}(T)$  dependence. Then, also taking into account the phonon scattering mechanism, the calculated dependence reproduces well the general trend in the apparent  $\mu_{\perp C}(T)$  dependence for the doped sample (Figure 6).

### 3.3. Electrical Conductivity Anisotropy

Physical properties of van der Waals materials are highly anisotropic due to the nature of their layered crystal structure [35–37]. Thus, in this work we investigated the variation of electrical conductivity in different crystallographic directions. For all the samples under investigation the transversal electrical conductivity is significantly lower than the longitudinal one and its variation with temperature exhibit semiconductor behavior (Figure 7, Table 3). In case of the Co-intercalated crystals, the electrical conductivity is lower than for the pristine one and is the lowest for the doped samples. The electrical conductivity anisotropy (ratio of longitudinal and transversal components) is the highest for the pristine *n*-type InSe and equals  $\sim 3.3 \times 10^3$  at  $T = 80 \text{ K}$  (Figure 8). Meanwhile, it decreases significantly with increasing temperature, namely by a factor of  $\sim 270$  in the temperature range from  $T = 80 \text{ K}$  to  $300 \text{ K}$ . The intercalation of cobalt decreases both the anisotropy ratio and the range of its variation in this temperature range. The lowest  $\sigma_{\perp C}/\sigma_{\parallel C}$  values are found for the doped samples, namely, at  $T = 80 \text{ K}$  the conductivity anisotropy decreased by more than a factor of 150 with respect to the pristine sample. It should be noted that to a large degree such low anisotropy values are due to the decrease in the longitudinal component but not to the increase in the transversal one.

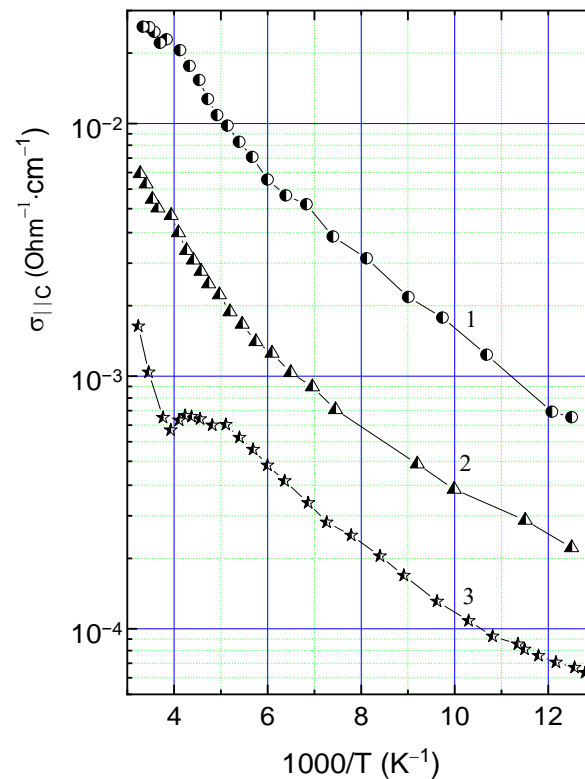


**Figure 7.** The out-of-plane electrical conductivity (i.e., across the van der Waals layers) versus temperature for as-grown pristine (1), Co-intercalated (2), and Co-doped (3) crystals of *n*-type InSe.

**Table 3.** Parameters of electrical conductivity anisotropy for different samples of *n*-type InSe.

Sample	Type of Sample	$\sigma_{\parallel C}, \text{ Ohm}^{-1}\cdot\text{cm}^{-1}$		$\sigma_{\perp C}/\sigma_{\parallel C}$		$\Delta E_b, \text{ meV}$	A(80 K)
		80 K	300 K	80 K	300 K		
1	Undoped	$6.87 \times 10^{-4}$	$2.42 \times 10^{-2}$	3265	12.3	41.9	7.5
2	Co-intercalated	$2.09 \times 10^{-4}$	$6.33 \times 10^{-3}$	151.3	7.62	19.1	9.5
3	Co-doped	$7.03 \times 10^{-5}$	$1.587 \times 10^{-3}$	19.6	6.29	16.6	1.8

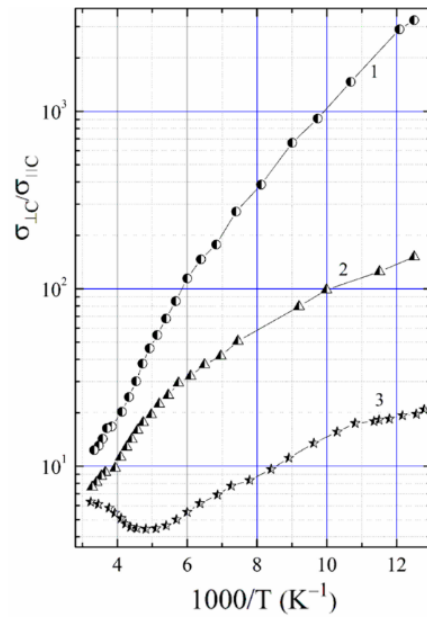


**Figure 8.** The electrical conductivity anisotropy versus temperature for as-grown pristine (1), Co-intercalated (2) and Co-doped (3) crystals of *n*-type InSe.

It was shown in [38] that the energy bands, which form the fundamental absorption edge of indium selenide are created with strong contribution of  $p_z$ -orbitals of selenium and have a 3D character, and even the component of longitudinal effective mass is higher than the transversal one ( $m_{\perp C}^* = 0.13m_0, m_{\parallel C}^* = 0.08m_0$ ). As a result, the apparent high anisotropy values should be related to defects. In layered materials, weak van der Waals bonding between neighboring layers promotes the formation of planar stacking faults between various structural polytypes. Such disordered ranges are places for aggregation of impurities and a reason for the appearance of energy barriers  $\Delta E_b$  between the layers which can explain activation dependence of the transversal conductivity:

$$\sigma_{\parallel C} = en\mu_{\parallel C} \exp(-\Delta E_b/kT), \tag{5}$$

and high values of the conductivity ratio

$$\sigma_{\perp C}/\sigma_{\parallel C} = A \exp(-\Delta E_b/kT) \tag{6}$$

The determined energy barrier value for the pristine crystal is the highest and equals  $\sim 42$  meV. For the samples intercalated and doped with Co the energy barrier decreases more than twice. The values of the preexponential factor  $A$  are evidently higher than the effective mass ratio ( $m_{\parallel C}^*/m_{\perp C}^* = 0.615$ ). It can be related to the high density of 2D electrons in all of the samples, which in contrast to three-dimensional (3D) carriers do not contribute to the charge carrier transfer across the InSe layers [39]. In this model, apart

from the barrier, the electrical conductivity anisotropy is also determined by relative values of the concentrations of 3D and 2D electrons and their mobilities:

$$\frac{\sigma_{\perp C}}{\sigma_{\parallel C}} = \frac{n_2 \mu_{2\perp C} + n_3 \mu_{3\perp C}}{n_3 \mu_{3\parallel C}} \exp(-\Delta E_b/kT). \quad (7)$$

It is high interest to investigate the layer thickness dependence of electrical properties of InSe with magnetic transition metal impurities at the two-dimensional limit down few-layer flakes in our next studies, as understanding of material properties of intercalated and doped few-layer thick van der Waals crystals holds enormous potential for the future development of applied and fundamental science [40–43]. We believe that our innovative approaches to intercalation and doping of van der Waals materials combined with high quality of the exfoliated few-layer fabrication process with promising properties will enable new routes in materials design to the low-dimensional magnetism.

#### 4. Conclusions

In conclusion, we have established that insertion of magnetic Co impurities in layered van der Waals crystals of *n*-type InSe by means of doping during crystal growth or by electrochemical intercalation of previously grown layered crystals has a significant effect on electrical parameters of this semiconductor material. Namely, this leads to a decrease in the free electron density, the Hall mobility  $\mu_{\perp C}$  along layers and the electrical conductivity anisotropy  $\sigma_{\perp C}/\sigma_{\parallel C}$ , as well as changing the metallic behavior of the  $\sigma_{\perp C}(T)$  dependence in the pristine sample into a semiconductor one. We also show that the interaction of electrons with space-charge regions is as an effective scattering mechanism and should be taken into account in Co-doped and intercalated InSe crystals. In both cases, the inserted magnetic impurity reveals the tendency to create clusters that is a result of low solubility of transition metals in InSe. Further developments of the crystal growth technique are required to incorporate substitutional transition metals in InSe in order to create a homogeneous magnetic crystal. Importantly, as revealed by our photoluminescence studies, the doped and intercalated InSe crystals remain optically, which enables optoelectronic applications of these materials. Our data and analysis indicate a route towards the controlled modulation of electron transport in hybrid systems, which integrate semiconducting and magnetic properties in the same material, offering opportunities for the development of novel device concepts. Since van der Waals materials are compatible with other van der Waals materials, dielectrics and magnetic metals, we envisage further developments and a new class of devices that exploit the magnetic properties of hybrid magnetic-semiconducting materials. Moreover, these findings will stimulate further research on magnetism in novel semiconductor materials beyond conventional Si and GaAs.

**Author Contributions:** Conceptualization, Z.D.K.; methodology, Z.D.K., I.V.M., P.I.S. and Z.D.K.; software, I.V.M.; validation, Z.D.K.; formal analysis, Z.R.K., I.V.M., P.I.S. and Z.D.K.; investigation, Z.R.K., I.V.M. and P.I.S.; resources, Z.R.K. and Z.D.K.; data curation, I.V.M. and P.I.S.; writing—original draft preparation, Z.R.K., I.V.M., P.I.S. and Z.D.K.; writing—review and editing, Z.R.K., I.V.M., P.I.S. and Z.D.K.; supervision, Z.D.K.; project administration, Z.D.K.; funding acquisition, Z.D.K. All authors have read and agreed to the published version of the manuscript.

**Funding:** This research was funded by the National Academy of Sciences of Ukraine, funding number III-14-19.

**Institutional Review Board Statement:** Not applicable.

**Informed Consent Statement:** Not applicable.

**Data Availability Statement:** All relevant data that support the findings of this study are available in Nottingham Research Data Management Repository (<http://doi.org/10.17639/nott.7245>).

**Conflicts of Interest:** The authors declare no conflict of interest.

## References

1. Ares, P.; Novoselov, K.S. Recent advances in graphene and other 2D materials. *Nano Mater. Sci.* **2022**, *4*, 3–9. [[CrossRef](#)]
2. Shanmugam, V.; Mensah, R.A.; Babu, K.; Gawusu, S.; Chanda, A.; Tu, Y.; Neisiany, R.E.; Försth, M.; Sas, G.; Das, O. A Review of the synthesis, properties, and applications of 2D Materials. *Part. Part. Syst. Charact.* **2022**, *39*, 2200031. [[CrossRef](#)]
3. Liang, G.; Wang, Y.; Zhang, J.; Kudrynskiy, Z.R.; Kovalyuk, Z.; Patanè, A.; Xin, Q.; Song, A. High-performance phototransistors by alumina encapsulation of a 2d semiconductor with self-aligned contacts. *Adv. Electron. Mater.* **2022**, *8*, 2100954. [[CrossRef](#)]
4. Venanzi, T.; Selig, M.; Pashkin, A.; Winnerl, S.; Katzer, M.; Arora, H.; Erbe, A.; Patanè, A.; Kudrynskiy, Z.R.; Kovalyuk, Z.D.; et al. Terahertz control of photoluminescence emission in few-layer InSe. *Appl. Phys. Lett.* **2022**, *120*, 092104. [[CrossRef](#)]
5. Buckley, D.; Kudrynskiy, Z.R.; Balakrishnan, N.; Vincent, T.; Mazumder, D.; Castanon, E.; Kovalyuk, Z.D.; Kolosov, O.; Kazakova, O.; Tzalenchuk, A.; et al. Anomalous low thermal conductivity of atomically thin InSe probed by scanning thermal microscopy. *Adv. Funct. Mater.* **2021**, *31*, 2008967. [[CrossRef](#)]
6. Mazumder, D.; Xie, J.; Kudrynskiy, Z.R.; Wang, X.; Makarovskiy, O.; Bhuiyan, M.A.; Kim, H.; Chang, T.-Y.; Huffaker, D.L.; Kovalyuk, Z.D.; et al. Enhanced optical emission from 2D InSe bent onto Si-pillars. *Adv. Opt. Mater.* **2020**, *8*, 2000828. [[CrossRef](#)]
7. Lv, Q.; Yan, F.; Mori, N.; Zhu, W.; Hu, C.; Kudrynskiy, Z.R.; Kovalyuk, Z.D.; Patanè, A.; Wang, K. Interlayer band-to-band tunneling and negative differential resistance in van der Waals BP/InSe field-effect transistors. *Adv. Funct. Mater.* **2020**, *30*, 1910713. [[CrossRef](#)]
8. Ubrig, N.; Ponomarev, E.; Zultak, J.; Domaretskiy, D.; Zólyomi, V.; Terry, D.; Howarth, J.; Gutiérrez-Lezama, I.; Zhukov, A.; Kudrynskiy, Z.R.; et al. Design of van der Waals interfaces for broad-spectrum optoelectronics. *Nat. Mater.* **2020**, *19*, 299–304. [[CrossRef](#)]
9. Kudrynskiy, Z.R.; Kerfoot, J.; Mazumder, D.; Greenaway, M.T.; Vdovin, E.E.; Makarovskiy, O.; Kovalyuk, Z.D.; Eaves, L.; Beton, P.H.; Patanè, A. Resonant tunnelling into the two-dimensional subbands of InSe layers. *Commun. Phys.* **2020**, *3*, 16. [[CrossRef](#)]
10. Bandurin, D.A.; Tyurnina, A.V.; Yu, G.L.; Mishchenko, A.; Zólyomi, V.; Morozov, S.V.; Kumar, R.K.; Gorbachev, R.V.; Kudrynskiy, Z.R.; Pezzini, S.; et al. High electron mobility, quantum Hall effect and anomalous optical response in atomically thin InSe. *Nat. Nanotechnol.* **2017**, *12*, 223–227. [[CrossRef](#)]
11. Bhuiyan, M.A.; Kudrynskiy, Z.R.; Mazumder, D.; Greener, J.D.G.; Makarovskiy, O.; Mellor, C.J.; Vdovin, E.E.; Piot, B.A.; Lobanova, I.I.; Kovalyuk, Z.D.; et al. Photoquantum Hall Effect and Light-Induced Charge Transfer at the Interface of Graphene/InSe Heterostructures. *Adv. Funct. Mater.* **2019**, *29*, 1805491. [[CrossRef](#)]
12. Kudrynskiy, Z.R.; Bhuiyan, M.A.; Makarovskiy, O.; Greener, J.D.G.; Vdovin, E.E.; Kovalyuk, Z.D.; Cao, Y.; Mishchenko, A.; Novoselov, K.S.; Beton, P.H.; et al. Giant Quantum Hall Plateau in Graphene Coupled to an InSe van der Waals Crystal. *Phys. Rev. Lett.* **2017**, *119*, 157701. [[CrossRef](#)] [[PubMed](#)]
13. Zhu, W.; Lin, H.; Yan, F.; Hu, C.; Wang, Z.; Zhao, L.; Deng, Y.; Kudrynskiy, Z.R.; Zhou, T.; Kovalyuk, Z.D.; et al. Large tunneling magnetoresistance in van der Waals ferromagnet/semiconductor heterojunctions. *Adv. Mater.* **2021**, *33*, 2104658. [[CrossRef](#)] [[PubMed](#)]
14. Gibertini, M.; Koperski, M.; Morpurgo, A.F.; Novoselov, K.S. Magnetic 2D materials and heterostructures. *Nat. Nanotechnol.* **2019**, *14*, 408–419. [[CrossRef](#)] [[PubMed](#)]
15. Ningrum, V.P.; Liu, B.; Wang, W.; Yin, Y.; Cao, Y.; Zha, C.; Xie, H.; Jiang, X.; Sun, Y.; Qin, S.; et al. Recent advances in two-dimensional magnets: Physics and devices towards spintronic applications. *Research* **2020**, *2020*, 1768918. [[CrossRef](#)] [[PubMed](#)]
16. Basnet, R.; Ford, D.; TenBerge, K.; Lochala, J.; Hu, J. Emergence of ferrimagnetism in Li-intercalated NiPS<sub>3</sub>. *J. Phys. Condens. Matter* **2022**, *34*, 434002. [[CrossRef](#)]
17. Kovalyuk, Z.D.; Boledzyuk, V.B.; Shevchyk, V.V.; Kaminskii, V.M.; Shevchenko, A.D. Ferromagnetism of layered GaSe semiconductors intercalated with cobalt. *Semiconductors* **2012**, *46*, 971–974. [[CrossRef](#)]
18. Bakhtinov, A.P.; Boledzyuk, V.B.; Kovalyuk, Z.D.; Kudrynskiy, Z.R.; Lytvyn, O.S.; Shevchenko, A.D. Magnetic properties and surface morphology of layered In<sub>2</sub>Se<sub>3</sub> crystals intercalated with cobalt. *Phys. Solid State* **2013**, *55*, 1148–1155. [[CrossRef](#)]
19. Boledzyuk, V.B.; Kovalyuk, Z.D.; Pyrlyya, M.N.; Shevchenko, A.D. Electrochemical, optical, and magnetic properties of Ni<sub>x</sub>InSe (0 < x ≤ 1) intercalation compounds. *Inorg. Mater.* **2014**, *50*, 976–980. [[CrossRef](#)]
20. Boledzyuk, V.B.; Kovalyuk, Z.D.; Kudrynskiy, Z.R.; Litvin, O.S.; Shevchenko, A.D. Structure and magnetic properties of cobalt-intercalated layered InSe crystals. *Tech. Phys.* **2014**, *59*, 1462–1465. [[CrossRef](#)]
21. Boledzyuk, V.B.; Kovalyuk, Z.D.; Kudrynskiy, Z.R.; Pyrlyya, M.N.; Feshak, T.N.; Shevchenko, A.D. Electrochemical, optical, and magnetic properties of Ni<sub>x</sub>GaSe (0 < x ≤ 1) intercalation compounds. *Inorg. Mater.* **2015**, *51*, 1086–1089. [[CrossRef](#)]
22. Boledzyuk, V.; Bakhtinov, A.; Kovalyuk, Z.; Kudrynskiy, Z.; Ivanov, V.; Slyn'ko, V. Preparation of nanocomposite magnetic compounds based on layered semiconductors by means of electrochemical intercalation in a gradient magnetic field. *Acta Phys. Pol. A* **2016**, *130*, 773–777. [[CrossRef](#)]
23. Slyn'ko, V.V.; Khandozhko, A.G.; Kovalyuk, Z.D.; Slyn'ko, V.E.; Zaslonskiy, A.V.; Arciszewska, M.; Dobrowolski, W. Ferromagnetic states in the InSe<sub>1-x</sub>Mn<sub>x</sub>Se layered crystal. *Phys. Rev. B* **2005**, *71*, 245301. [[CrossRef](#)]
24. Lashkarev, G.V.; Sichkovskiy, V.I.; Radchenko, M.V.; Karpina, V.A.; Butorin, P.E.; Dmitriev, O.I.; Lazorenko, V.I.; Slyn'ko, E.I.; Lytvyn, P.M.; Jakiela, R.; et al. Diluted magnetic semiconductors based on II–VI, III–VI, and IV–VI compounds. *Low Temp. Phys.* **2009**, *35*, 62–70. [[CrossRef](#)]

25. Lashkarev, G.V.; Sichkovskiy, V.I.; Radchenko, M.V.; Aleshkevych, P.; Dmitriev, O.I.; Butorin, P.E.; Kovalyuk, Z.D.; Szymczak, R.; Slawska-Waniewska, A.; Nedelko, N.; et al. Diluted magnetic layered semiconductor InSe:Mn with high Curie temperature. *Semicond. Phys. Quantum Electron. Optoelectron.* **2011**, *14*, 263–268. [[CrossRef](#)]
26. Moro, F.; Bhuiyan, M.A.; Kudrynskiy, Z.R.; Puttock, R.; Kazakova, O.; Makarovskiy, O.; Fay, M.W.; Parmenter, C.; Kovalyuk, Z.D.; Fielding, A.J.; et al. Room temperature uniaxial magnetic anisotropy induced by Fe-islands in the InSe semiconductor van der Waals crystal. *Adv. Sci.* **2018**, *5*, 1800257. [[CrossRef](#)] [[PubMed](#)]
27. El-Sayed, K.; Heiba, Z.K.; Sedeek, K.; Hantour, H.H. Magnetic, electric and crystallographic properties of diluted magnetic InSe<sub>(1-x)</sub>Fe(Co)<sub>x</sub> semiconductor. *J. Alloys Compd.* **2012**, *530*, 102–106. [[CrossRef](#)]
28. Lashkarev, G.V.; Slynko, V.V.; Kovalyuk, Z.D.; Sichkovskiy, V.I.; Radchenko, M.V.; Aleshkevych, P.; Szymczak, R.; Dobrowolski, W.; Minikaev, R.; Zasloukin, A.V. Anomalies of magnetic properties of layered crystals InSe containing Mn. *Mater. Sci. Eng. C* **2007**, *27*, 1052–1055. [[CrossRef](#)]
29. Rigoult, J.; Rimsky, A.; Kuhn, A. Refinement of the 3R  $\gamma$ -indium monoselenide structure type. *Acta Crystallogr. Sect. B* **1980**, *36*, 916–918. [[CrossRef](#)]
30. Segura, A.; Wünnel, K.; Chevy, A. Investigation of impurity levels in n-type indium selenide by means of Hall effect and deep level transient spectroscopy. *Appl. Phys. A* **1983**, *31*, 139–145. [[CrossRef](#)]
31. Schmid, P. Electron-lattice interaction in layered semiconductors. *Il Nuovo Cim. B (1971–1996)* **1974**, *21*, 258–270. [[CrossRef](#)]
32. Savitskiy, P.I.; Kovalyuk, Z.D.; Mintyanskiy, I.V. Space-charge region scattering in indium monoselenide. *Phys. Status Solidi A* **2000**, *180*, 523–531. [[CrossRef](#)]
33. Zasloukin, A.V.; Kovalyuk, Z.D.; Mintyanskiy, I.V.; Savitskiy, P.I. Electrical properties of fast cooled InSe single crystals. *Semicond. Phys. Quantum Electron. Optoelectron.* **2008**, *11*, 54–58. [[CrossRef](#)]
34. Weisberg, L.R. Anomalous mobility effects in some semiconductors and insulators. *J. Appl. Phys.* **1962**, *33*, 1817–1821. [[CrossRef](#)]
35. Kim, S.E.; Mujid, F.; Rai, A.; Eriksson, F.; Suh, J.; Poddar, P.; Ray, A.; Park, C.; Fransson, E.; Zhong, Y.; et al. Extremely anisotropic van der Waals thermal conductors. *Nature* **2021**, *597*, 660–665. [[CrossRef](#)] [[PubMed](#)]
36. Suzuki, M.; Gao, B.; Shibata, G.; Sakamoto, S.; Nonaka, Y.; Ikeda, K.; Chi, Z.; Wan, Y.X.; Takeda, T.; Takeda, Y.; et al. Magnetic anisotropy of the van der Waals ferromagnet Cr<sub>2</sub>Ge<sub>2</sub>Te<sub>6</sub> studied by angular-dependent x-ray magnetic circular dichroism. *Phys. Rev. Res.* **2022**, *4*, 013139. [[CrossRef](#)]
37. Shu, H. Highly-anisotropic carrier transport and optical properties of two-dimensional titanium trisulfide. *J. Mater. Sci.* **2022**, *57*, 3486–3496. [[CrossRef](#)]
38. Gomes da Costa, P.; Dandrea, R.G.; Wallis, R.F.; Balkanski, M. First-principles study of the electronic structure of g-InSe and B-InSe. *Phys. Rev. B* **1993**, *48*, 14135–14141. [[CrossRef](#)]
39. Pomer, F.; Bonet, X.; Segura, A.; Chevy, A. Electrical conductivity anisotropy in tin-doped n-type indium selenide. *Phys. Status Solidi B* **1988**, *145*, 261–268. [[CrossRef](#)]
40. Guo, Z.; Zeng, Y.; Meng, F.; Qu, H.; Zhang, S.; Hu, S.; Fan, S.; Zeng, H.; Cao, R.; Prasad, P.N.; et al. In-situ neutron-transmutation for substitutional doping in 2D layered indium selenide based phototransistor. *eLight* **2022**, *2*, 9. [[CrossRef](#)]
41. Zhang, X.; Liu, W.; Niu, W.; Lu, Q.; Wang, W.; Sarikhani, A.; Wu, X.; Zhu, C.; Sun, J.; Vaninger, M.; et al. Self-intercalation tunable interlayer exchange coupling in a synthetic van der Waals antiferromagnet. *Adv. Funct. Mater.* **2022**, *32*, 2202977. [[CrossRef](#)]
42. Liu, Y.; Hu, Z.; Tong, X.; Bauer, E.D.; Petrovic, C. Electrical and thermal transport in van der Waals magnets 2H-M<sub>x</sub>TaS<sub>2</sub> (M = Mn, Co). *Phys. Rev. Res.* **2022**, *4*, 013048. [[CrossRef](#)]
43. Wang, Y.; Jiang, S.; Xiao, J.; Cai, X.; Zhang, D.; Wang, P.; Ma, G.; Han, Y.; Huang, J.; Watanabe, K.; et al. Ferroelectricity in hBN intercalated double-layer graphene. *Front. Phys.* **2022**, *17*, 43504. [[CrossRef](#)]